Optical Engineering

OpticalEngineering.SPIEDigitalLibrary.org

Enhanced performance of refractive laser beam shapers through additional phase control at focus

Meijie Li
Youri Meuret
Michael Vervaeke
Hugo Thienpont
Fabian Duerr

SPIE.

Meijie Li, Youri Meuret, Michael Vervaeke, Hugo Thienpont, Fabian Duerr, "Enhanced performance of refractive laser beam shapers through additional phase control at focus," *Opt. Eng.* **55**(8), 085106 (2016), doi: 10.1117/1.OE.55.8.085106.

Enhanced performance of refractive laser beam shapers through additional phase control at focus

Meijie Li,[a,*] Youri Meuret,[a,b] Michael Vervaeke,[a] Hugo Thienpont,[a] and Fabian Duerr[a]
[a]Vrije Universiteit Brussel, Faculty of Engineering, Applied Physics and Photonics Department TONA, Brussels Photonics Team (B-PHOT), Pleinlaan 2, Brussels 1050, Belgium
[b]KU Leuven, Light and Lighting Laboratory, Gebroeders De Smetstraat 1, Gent 9000, Belgium

Abstract. Laser beam shaping at focus or focal beam shaping is essential for many applications. The most common approach makes use of the Fourier transforming properties of lenses to generate at their focal planes the desired irradiance patterns, e.g., the flattop. There are two inherent limitations for this approach. First, the shaping quality depends strongly on the dimensionless parameter β. In the case of a long focal length or small beam sizes giving a small β value, additional beam expanders are needed to achieve a satisfying irradiance pattern at the focus. Second, without considering the phase, the irradiance patterns beyond the focal plane are not controlled. We propose a different approach with two plano-aspheric lenses that allow control of both irradiance and phase at focus. The design method comprises an extended ray mapping procedure combined with backward wave propagation from focus. With this design approach, the shaping quality is guaranteed without the possible need for extra beam expanders, offering the potential for a more compact system with fewer elements. Through the additional phase control, the depth of focus is enlarged to a large extent and the designed system becomes more tolerant. [DOI: 10.1117/1.OE.55.8.085106]

Keywords: laser beam shaping; lens system design; geometric optical design; aspherics; laser focus; wave propagation.

Paper 160446P received Mar. 25, 2016; accepted for publication Aug. 12, 2016; published online Aug. 29, 2016.

1 Introduction

Laser beam shaping at focus, often referred to as focal beam shaping (FBS), is widely used in many laser applications, such as laser material processing, medical operations, optical processing, optical data storage, laser printing, and laser research.[1] FBS means that the laser beam is focused to a small area to have a sufficiently high-power density, and in the meantime is shaped to obtain a desired irradiance pattern (often a flattop) at the focal plane to achieve optimum system performance.

In general, a collimated beam shaper,[2,3] or more often a phase element[4,5] is combined with a lens to generate a focal beam with the desired irradiance pattern at the focal plane of the lens. These FBS approaches make use of the Fourier transforming properties of lenses. The approach combining the phase element with the Fourier lens is illustrated in Fig. 1.[4] The input beam is a collimated single-mode laser beam with a Gaussian irradiance distribution. The phase element can either be refractive or diffractive optics, which modifies the phase of the beam. The transform element is the lens that generates the Fourier transform of the optical field with the modified phase at its focal plane. This approach will be referred to as the "Fourier approach" throughout this paper.

There are different methods available to calculate the phase of the phase element, including the geometrical optics-based method,[4] the stationary phase method,[5] the iterative method,[6] and the optimization-based method.[7] All these methods can control only the irradiance but not the phase at the focal plane. Without the phase control, the generated irradiance pattern degrades quickly beyond the focal plane.[8] For certain cases, there is even a much more focused spot found in the vicinity of the focal plane, which is highly detrimental for deep or bulk laser micromachining applications.[9] Hence the phase at the focal plane is better to be controlled to be constant. The common solution is to add a second phase element at the focal plane to correct the phase to obtain a collimated beam.[8,9] The alignment of such a phase correcting element can be quite demanding.

There is another drawback for the Fourier approach. The quality of the irradiance pattern that can be obtained strongly depends on the dimensionless parameter β.[4,5,10–13]

$$\beta = \frac{C r_o R_o}{\lambda f}, \tag{1}$$

where C is a constant, r_o is the radius of the input laser beam, R_o is the radius of the output beam at the focal plane, λ is the design wavelength, and f is the focal length of the Fourier transform lens or the distance from the FBS system to the focal plane. In literature, C has been chosen to be either 2π[5] or $2\sqrt{2\pi}$[4,10–13] for calculation convenience. In the following discussions, we have chosen $C = 2\sqrt{2\pi}$ as is mostly used in the case of shaping a Gaussian beam to have the flattop profile at focus.

The impact of β on the shaping quality for the circular flattop pattern at focus is illustrated in Fig. 2. The solid line is the cross section of the targeted pattern described by a step function. The dotted lines show results for different β values by changing the radius of the input laser beam. These simulation results have been obtained using the unified optical modeling software "VirtualLab," and they agree

*Address all correspondence to: Meijie Li, E-mail: mli@b-phot.org

0091-3286/2016/$25.00 © 2016 SPIE

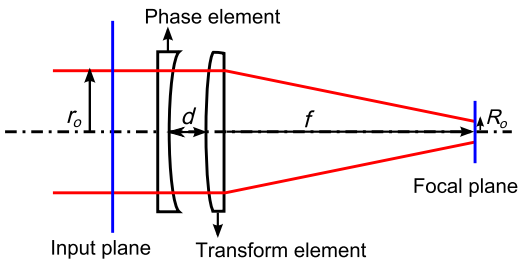

Fig. 1 Schematic drawing of the FBS system based on the Fourier transform lens. The phase element is the beam shaping element, which modifies the phase of the collimated input light beam. The transform element is a Fourier transform lens, which generates the Fourier transform of the modified optical field at the focal plane.

very well with the reported figures in literature.[4,12,13] With a decreasing β value, deviations from the ideal flattop shape begin to appear. Depending on what might be considered as still sufficiently close to a flattop distribution, a threshold value for β can be defined, e.g., $\beta = 4$. For β values smaller than this threshold, the beam shaping system will not deliver acceptable results.

In practice, the laser wavelength λ, the spot radius at focus R_o, and the working distance or the focal length f are typically determined by the considered applications. In case of a too small β value, the only possibility is to expand the initial laser beam so that the newly obtained β will be large enough to provide the irradiance profile sufficiently close to the target. A typical solution is shown in Fig. 3, where a two-lens telescope has been added to expand the input laser beam. However, these additional optical elements make the complete system less compact with more elements to be aligned. It should be stressed that for targeted irradiance distributions other than the flattop, the threshold value of β can be significantly higher than 4 to still obtain satisfactory beam shaping results.[4]

In this work, we present a different approach that uses two plano-aspheric lenses to control both irradiance and phase at laser focus with no need for an additional phase correcting element at the focal plane. It is called the "added-phase-control approach." This design strategy and method does not rely on the Fourier transforming properties of lenses and is explained in Sec. 2. In Sec. 3, the added-phase-control

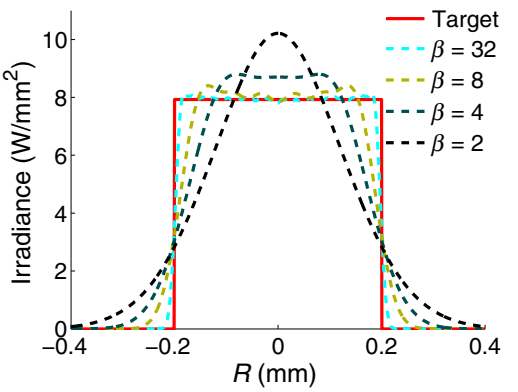

Fig. 2 The cross-section profiles of the circular irradiance patterns generated by the Fourier approach. The design target is a flattop pattern with sharp edges at focus. It requires β to be large enough in order to have the irradiance profile sufficiently close to the target.

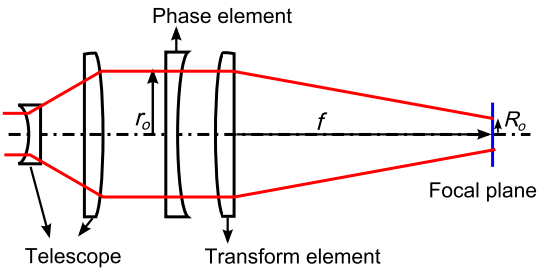

Fig. 3 A practical solution to enlarge β for the Fourier approach is to add a two-lens telescope to expand the input laser beam.

approach is applied for a design task to transform an input Gaussian beam to a circular flattop profile at focus with a small initial β value. In contrast to the Fourier approach, our developed added-phase-control approach does not require additional elements to expand the input laser beam. In Sec. 4, we present a comprehensive sensitivity analysis to highlight several additional practical benefits of our approach and to demonstrate the added value of the direct phase control at focus.

2 Direct Design Approach to Control Both Irradiance and Phase at Laser Focus

The designed two-lens FBS system is schematically shown in Fig. 4. In literature, the existing direct design methods to control only the irradiance at focus are based on either geometrical optics or diffraction theory. We have introduced the intermediate plane at the exit of the shaping optics to combine both geometrical optics and wave optics, which allows to control both irradiance and phase at the focal plane. First, the required optical field at the focus is propagated backward to the intermediate plane using proper wave propagation method from diffraction theory.[14] Then the field information at the intermediate plane is translated to ray information, so that the ray mapping technique[15] can be extended to design the two lenses.

The design procedure can be divided into two steps.

2.1 *Step I: Backward Propagation From the Focal Plane to the Intermediate Plane*

The optical field at the focal plane is defined to have the required irradiance distribution and the constant phase,

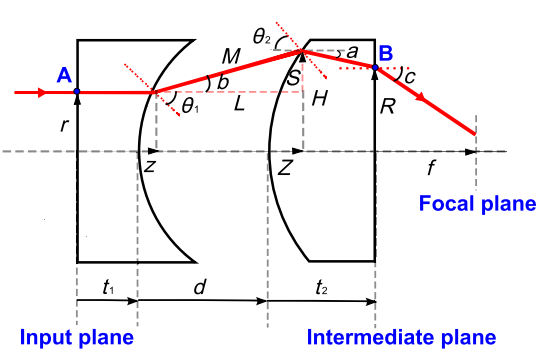

Fig. 4 Schematic drawing of the FBS system with two plano-aspheric lenses used in the added-phase-control approach. An arbitrary ray (in red) intersects the input plane at radius, r, goes through the intermediate plane at radius, R, and then arrives at the focal plane at a distance f from the output plane.

and is then propagated back to the intermediate plane in free space using wave propagation methods. Depending on the focal spot size and the propagation distance, different propagation methods from diffraction theory[14] can be used, including the method of angular spectrum of plane waves (SPWs), the Fresnel propagation method, and the Fraunhofer propagation method. In our case, we have performed the backward propagation in VirtualLab by using the SPW operator, but any other suitable software or programming language could also be used. SPW operator is based on the rigorous propagation method of angular SPWs, and the number of the sampling points is defined large enough to ensure good accuracy. The field at the focal plane can be described either by analytical functions or discrete data points. The field information that can be extracted is numerical data.

Suppose the radial coordinate at the intermediate plane is R, the obtained field information includes the irradiance $I(R)$ and the phase $\Phi(R)$. For calculation convenience, $I(R)$ is normalized so that the total power is 1 W, and $\Phi(0)$ equals to 0 by taking the point on the optical axis as the reference.

The obtained field information at the intermediate plane can now be translated to the ray information that is needed to design the lenses. In Fig. 4, the path of an arbitrary ray is highlighted in red. For each ray, the necessary information at the intermediate plane is the ray position R, the ray direction angle $c(R)$, and the optical path length (OPL) difference with respect to the on-axis ray $\mathrm{OPD}(R)$. Due to the rotational symmetry of the considered optical system, it is sufficient to consider only $R \geq 0$. Then the direction angle is calculated as

$$c(R) = a \sin\left(-\frac{\Phi'(R)}{k}\right), \tag{2}$$

where k is the wave number. The OPL difference is calculated as

$$\mathrm{OPD}(R) = \frac{\Phi(R)}{k}. \tag{3}$$

2.2 *Step II: Lens Design by Ray Mapping From the Input Plane to the Intermediate Plane*

Design of double freeform surfaces for laser beam shaping has been investigated over the years. However, detailed design procedures have been reported mainly for collimated laser beam shaping with plane wavefronts.[15–24] There is work[25] which can be used to generate a freeform wavefront; however, the irradiance is defined in the case at a plane close to the wavefront rather than on the wavefront itself. In our case, we have defined both the irradiance and the phase at the same plane, so that the design has a good accuracy even when the beam is strongly focused.

Figure 4 introduces all the necessary parameters for the optical design process. For the first lens, the radial coordinates at both surfaces are the same as r. For the second lens, the first surface has the radial coordinate H, while the second surface's radial coordinate is R. To make the design adaptable to both magnifying and demagnifying systems, the signs of certain parameters should be taken into account. The sag values z and Z of two aspherical surfaces are defined positive if the corresponding surface point is at the right side of the on-axis point, otherwise the value is negative. The slope values v and V are defined as

$$v = \tan(\theta_1), \quad V = \tan(\theta_2), \tag{4}$$

where θ_1 and θ_2 are positive when the surface normal is below the forward horizon as plotted. Otherwise, they have negative values. Similar definitions apply for the angles a and c. For angle b, the sign definition is in the opposite way for calculation convenience.

Supposing there is no energy loss in the beam shaping system, the radial coordinates r and R can be mapped to each other based on the theory of energy conservation. As the irradiance at the intermediate plane $I(R)$ has already been normalized, the irradiance at the input plane $I_{\mathrm{in}}(r)$ should also be normalized so that

$$2\pi \int_0^{\infty} r I_{\mathrm{in}}(r)\mathrm{d}r = 1. \tag{5}$$

To map r and R, the encircled energy within r at the input plane should be the same with that within R at the intermediate plane as

$$2\pi \int_0^{r} x I_{\mathrm{in}}(x)\mathrm{d}x = 2\pi \int_0^{R} x I(x)\mathrm{d}x. \tag{6}$$

By applying the Snell's law on each refractive surface, the angles can be related to one another by the following equations:

$$n \sin(\theta_1) = \sin(\theta_1 + b), \tag{7}$$

$$\sin(\theta_2 + b) = n \sin(a - \theta_2), \tag{8}$$

$$n \sin(a) = \sin(c), \tag{9}$$

where n is the refractive index of the material of the two lenses. The slope values v and V can now be derived from Eqs. (7) and (8), respectively, as follows

$$v = \tan(\theta_1) = \frac{\sin(b)}{n - \cos(b)}, \tag{10}$$

$$V = \tan(\theta_2) = \frac{\sin(b) + n \sin(a)}{n \cos(a) - \cos(b)}. \tag{11}$$

As in the triangle $L - M - S$ where $\sin(b) = (S/M)$ and $\cos(b) = (L/M)$, the slope equations can be rewritten as

$$v = \frac{S}{nM - L}, \tag{12}$$

$$V = \frac{S + nM \sin(a)}{nM \cos(a) - L}. \tag{13}$$

Having d as the separation between two lenses and t_2 as the thickness of the second lens, the triangle $L - M - S$ can be calculated as below:

$$L = d - z + Z, \tag{14}$$

$$S = (t_2 - Z)\tan(a) + R - r, \tag{15}$$

$$M = \sqrt{L^2 + S^2}. \tag{16}$$

Last but not least, the OPL from the input plane to the intermediate plane should be calculated. For the center ray on axis

$$\mathrm{OPL}_0 = nt_1 + d + nt_2. \tag{17}$$

For any other ray

$$\mathrm{OPL} = N(t_1 + z) + M + n\left(\frac{t_2 - Z}{\cos(a)}\right). \tag{18}$$

As the OPL difference at the input plane is 0, the OPL difference from the two equations above is the same as that in Eq. (3). So that

$$\frac{\Phi}{k} = n\left(z - t_2 + \frac{t_2 - Z}{\cos(a)}\right) + M - d. \tag{19}$$

It should be noticed that t_1 is eliminated, hence the design does not depend on the thickness of the first lens t_1. To calculate the lenses' surfaces, it is only necessary to specify the wavelength λ or the wave number k, the refractive index n, the lens separation d, and the thickness of the second lens t_2.

Next, the design procedure is explained step by step as follows:

- Step 1: As our calculation is based on numerical data, the maximum dimensions of r and R should be defined. $r_{\max}$ and $R_{\max}$ are both defined by the total energy passing through the system. In our case, we have selected the clear aperture $r_{\max}$ to be $3r_o$ to avoid truncation effects.[10]
- Step 2: According to our previous work,[24] the radial coordinates r and R should be sampled by equal distant bins as

$$r_i = 0, \frac{r_{\max}}{p}, 2\frac{r_{\max}}{p}, \ldots, r_{\max}, \tag{20}$$

$$R_i = 0, \frac{R_{\max}}{q}, 2\frac{R_{\max}}{q}, \ldots, R_{\max}, \tag{21}$$

  where i is the counting index, and p and q are the number of bins for r and R, respectively.
- Step 3: Some parameters are dependent on R only. $\Phi(R)$ is obtained from Sec. 2.1. The refraction angle at the last refractive surface $c(R)$ is given by Eq. (2). The angle $a(R)$ is then calculated according to Eq. (9). Following Eq. (6), R can be expressed as a function of r as $R(r)$, therefore, these parameters can be also written as $\Phi(r)$, $c(r)$, and $a(r)$.
- Step 4: To calculate the sag value of the first aspheric surface z, a first-order differential equation is expected in the format below

$$\frac{dz}{dr} = v(r, z). \tag{22}$$

  From Eq. (12), the slope v is a function of (L, M, S) which depends on $[r, R(r), a(r), z, Z]$ according to Eqs. (14–16). This means that both v and M can be written as functions of (r, z, Z). Substituting $R(r)$, $\Phi(r)$, $a(r)$, $M(r, z, Z)$ into the Eq. (19), we can derive Z as a function of (r, z). Hence, we can have the slope v as $v(r, z)$ to have the expected Eq. (22). This equation is then solved for r_i to have z_i. We have chosen the ordinary differential equation (ODE) solver "ode45" in MATLAB® using the Runge–Kutta methods.
- Step 5: The slope of the first surface v_i is calculated according to the function $v(r, z)$ in the last step.
- Step 6: Similar to step 4, the following equation is expected to calculate the sag of the second aspheric surface Z:

$$\frac{dZ}{dR} = V(R, Z). \tag{23}$$

  From Eq. (13), the slope V is a function of $[L, M, S, a(R)]$. According to Eqs. (14)–(16), (L, M, S) depends on $[r, R, a(R), z, Z]$. Following Eq. (6), r can be obtained from R as $r(R)$. So both V and M can be written as functions of (R, z, Z). Substituting $r(R)$, $\Phi(R)$, $a(R)$, and $M(R, z, Z)$ into Eq. (19), we can derive z as a function of (R, Z). Hence, we can have the slope V as $V(R, Z)$ to have the expected Eq. (23). This equation is then solved for R_i to have Z_i in the same way as in step 4.
- Step 7: The slope of the first surface V_i is calculated according to the function $V(R, Z)$ in the last step.
- Step 8: It should be noticed that the radial coordinate of the second aspheric surface is not R but H, which can be calculated as

$$H = (t_2 - Z)\tan(a) + R. \tag{24}$$

  Following Eq. (24), H_i and $H_{\max}$ can be calculated from R_i and $R_{\max}$.

In the end, we have the full information to describe the two aspheric surfaces with (r_i, v_i, z_i) for the aspheric surface of the first lens and (H_i, V_i, Z_i) for the aspheric surface of the second lens.

3 Design Example: From Gaussian to Circular Flattop Pattern at Focus

Although our developed added-phase-control approach in Sec. 2 is not limited to a flattop profile at focus, we have selected this design example as it is the most commonly used design example in case of the Fourier approach.

The input beam is a single-mode He–Ne laser beam which has its waist at the input plane of the beam shaper, so the irradiance distribution is Gaussian, described as

$$I_{\mathrm{in}}(r) = \frac{2}{\pi r_o^2}\exp\left(-2\frac{r^2}{r_o^2}\right), \tag{25}$$

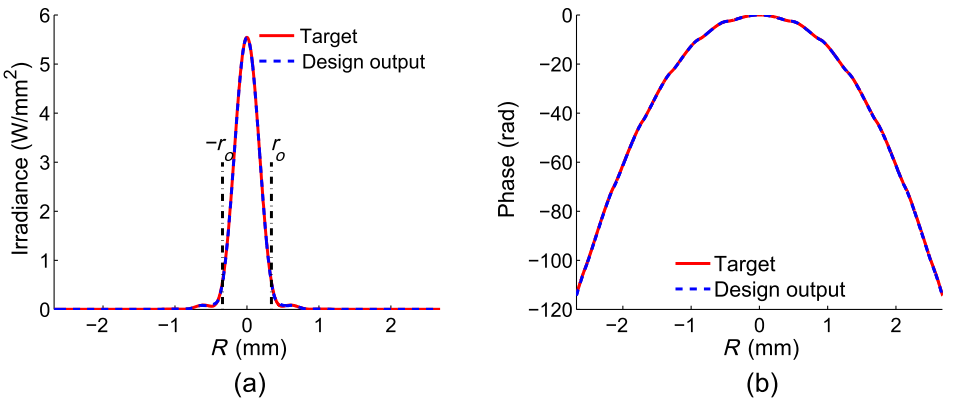

Fig. 5 The field information at the intermediate plane for having the flattop profile at focus: (a) irradiance and (b) phase. The design output (in blue) from simulation in VirtualLab fits well with the target (in red) calculated by the backward propagation. The reference $r_o = 0.34$ mm is the input beam radius.

where r_o is the beam radius within which the encircled energy is 86%. The flattop profile at the focal plane is chosen to have roll-off edges rather than perfect steep ones to avoid strong ripples in the far-field diffraction pattern.[18] Shealy and Hoffnagle[26] have summarized for laser beam shaping different flattened profiles, from which we have selected a commonly used one Fermi–Dirac (FD) profile described as

$$I_{\mathrm{FD}}(R) = I_{\mathrm{FD}}\left\{1 + \exp\left[\beta_{\mathrm{FD}}\left(\frac{R}{R_o} - 1\right)\right]\right\}^{-1}, \tag{26}$$

where I_{FD} is the constant to have normalized total power and R_o is the characteristic radius, where the irradiance is $0.5I_{\mathrm{FD}}$. β_{FD} should be properly selected to ensure not only a flattened profile but also one without too steep edges. We have chosen $\beta_{\mathrm{FD}} = 16.25$ as proposed in literature.[18,26]

As discussed in Sec. 1, the difficulty of obtaining the expected focal spot shape increases with reduced focal spot sizes and/or increased focal lengths, in cases where the input beam is given and has a fixed size at the beam shaper. For our design, with the fixed input radius $r_o = 0.34$ mm and wavelength $\lambda = 632.8$ nm, the output radius R_o is selected rather small as 0.2 mm and the focal length f is chosen relatively long as 269.2 mm. There are some applications, such as laser additive manufacturing, requiring such small focal spot sizes for high fabrication resolutions and high-power densities, and meanwhile long working distances to avoid damages on optics by backscattering from the fabrication process. However, the resulting $\beta = 2$ for the Fourier approach means that it is not possible to have a good shaping quality of the generated flattop profile without additional beam expansions.

With our added-phase-control approach, the beam size is not necessarily maintained from the first lens to the second lens, while the Fourier approach has the same beam size on the shaping element and the transform element. So Eq. (1) should not be directly applied for the added-phase-control approach. It makes more sense to slightly modify the calculation of β by using r_o as the radius at the intermediate plane rather than at the input plane, as the field propagation is performed between the intermediate plane and the focal plane. The field information at the intermediate plane for this specific design example is shown in Fig. 5. The red solid lines are the design targets directly obtained from the backward propagation, and the blue dashed lines are the simulation results for our design, which fit well to the targets. For the irradiance distribution in Fig. 5(a), the beam radius $r_{o'}$ is 0.37 mm, supposing that it is defined as the radius within which the encircled energy is 86%. Referring to the input radius $r_o = 0.34$ mm, there is a slight internal beam expansion by the designed beam shaper, increasing β' to 2.18, which is still clearly smaller than the $\beta = 4$ for which the Fourier approach already shows derivations from the target. For the phase distribution in Fig. 5(b), the design output agrees very well with the target, even for such a strongly focused beam.

For our design with the added-phase-control approach, poly (methyl methacrylate) (PMMA) with the refractive index 1.489 is selected as the lens material. The main reason for this choice is that we plan to fabricate a proof-of-concept prototype using ultra-precision diamond tooling (UDT),[27] and PMMA is one popular type of diamond turntable material. Depending on specific application requirements, other lens materials could be used as well by adapting the refractive index in the design algorithm. To ensure that the designed lenses are feasible for fabrication and assembly, several design parameters should be carefully selected. The first parameter is the lens separation d. For a larger lens separation d, the tolerance on d for lens assembly improves, and the slope values and aspheric departure of the designed aspherical surfaces decrease which typically eases the lens fabrication. Here, the aspheric departure is on the order of several micrometers. However, the surface sag values decrease as well and there is normally a lower limit for the sag values for the lens fabrication. Therefore, we have chosen a compromise value of $d = 100$ mm. Second, the thickness all over the lens aperture should not be smaller than 5 mm, which can be controlled by specifying a proper center thickness of the lenses t_1 and t_2. The full prescription of the lens system is summarized as follows:

- the refractive index of the lens material: $n = 1.489$;
- the lens separation: $d = 100$ mm;
- the center thickness of the two lenses: $t_1 = 5$ mm and $t_2 = 5.1$ mm; and
- the clear apertures of the two lenses: $r_{\max} = 2.0637$ mm and $H_{\max} = 6.7562$ mm.

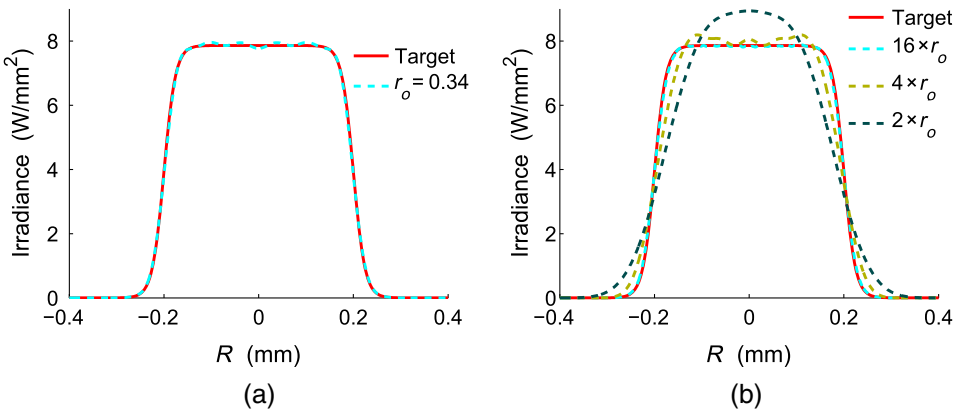

Fig. 6 The cross-section profiles for the circular FD pattern at focus: (a) for the added-phase-control approach, the design output fits well with the target without the need of external beam expansions and (b) or the Fourier approach, the input beam has to be expanded by at least 16 times to match the shaping quality of the added-phase-control approach.

To verify the design, the complete system from the input plane to the focal plane is simulated in VirtualLab, where the SPW operator is used to simulate the wave propagation from the intermediate plane to the focal plane to include diffraction effects. The simulated irradiance profile at the focal plane is given in Fig. 6(a). By having the input beam radius $r_o = 0.34$ mm directly at the input plane, the flattop profile can be well maintained.

For the same application, we have also tested the Fourier approach by using the solution shown in Fig. 3 to enlarge β. The telescope is formed by two ideal lenses with the first one negative and the second one positive. The phase element is assumed to be a plano-aspheric lens with very thin center thickness 1 μm, and the thickness of the lens varies to fit the required phase. The transform element is assumed to be an ideal lens with the required focal length f. The separation d is also very small in the range of a few micrometers to hundreds of micrometers which is just enough to have no overlaps between the two elements. The simulation results in Fig. 6(b) show that the external beam expansion has to be 16 times, increasing β from 2 to 32, so that the achieved beam shaping quality starts to match the result obtained with our added-phase-control approach. This result underlines the necessity to use an extra beam expanding system in the case where the initial β value is not large enough.

4 Sensitivity Analysis: the Added-Phase-Control Approach Versus the Fourier Approach

It is well known that refractive beam shapers as one kind of field mappers are very sensitive to variations of input laser beam parameters,[4,10] therefore, a tolerant design is very important for a good shaping quality in practical applications. Furthermore, several FBS applications, such as laser drilling and photowriting in the bulk of a material, require a large depth of focus.[9] In this section, we will compare our proposed added-phase-control approach with the Fourier approach by analyzing the system's sensitivity toward the displacement of the detector from the focal plane, the radius change, and the lateral shift of the input laser beam. For the added-phase-control approach, the design in Sec. 3 is directly used. For the Fourier approach, the design with $\beta = 32$, as in Sec. 3, is selected for comparison, as it has the similar shaping quality for the same design task. The telescope is formed by two ideal lenses with focal lengths $f_1 = -25$ mm and $f_2 = 400$ mm and a lens separation $f_1 + f_2$. The original laser beam with $r_o = 0.34$ mm has its waist at 25 mm ahead of the first lens, while the input plane of the beam shaper is placed at 400 mm after the second lens. It should be noticed that other combinations of telescope lenses give very similar results, as all the used lenses are assumed to be ideal.

To evaluate the shaping quality, the difference between the actual irradiance and the expected one can be quantified by the relative root-mean-squared error (RRMSE)[25,28]

$$\mathrm{RRMSE} = \sqrt{\frac{1}{Ns}\sum_{k=1}^{Ns}\left(\frac{I_{\mathrm{ak}} - I_{\mathrm{tk}}}{I_{\mathrm{tk}}}\right)^2}. \tag{27}$$

As the irradiance pattern is rotationally symmetric, the calculation is performed only for the cross-section profile. Ns is the sampling points and k is the index of the detection points. I_{ak} and I_{tk} are the actual and targeted irradiances on the k'th point, respectively. For the FD profile with $R_o = 0.2$ mm at focus, the physical dimension to be analyzed is defined from -0.2 to 0.2 mm with the number of sampling points $Ns = 501$. For the FD profile achieved by the added-phase-control approach in Fig. 6(a), it matches the target well, which is also underlined by a low RRMSE value of 0.0117. For the FD profiles generated by the Fourier approach in Fig. 6(b), clear derivation between the target and the design result can be observed with RRMSE = 0.0809 for $\beta = 8$, and in the case of $\beta = 4$, RRMSE is 0.2612 giving a profile that is no longer a flattop. Referring to the profiles in Fig. 6 with different RRMSE values, we have set 0.045 as the RRMSE limit below which the generated profile is considered to be in good agreement with the target, and the shaping quality is considered excellent when RRMSE is smaller than 0.025. Other limit values could also be set, as long as they are used consistently for the comparisons.

The sensitivity toward different parameter variations to have both good and excellent shaping qualities is summarized in Table 1, and the simulated irradiance profiles influenced by different variations are given in Fig. 7. Our added-phase-control approach demonstrates the following advantages in direct comparison with the Fourier approach.

Table 1 Sensitivity analysis for different parameter variations for the design example in Sec. 3: I the added-phase-control approach is compared with II the Fourier approach with $\beta = 32$. RRMSE = 0.045 is the limit for good shaping quality, and 0.025 is the limit for excellent shaping quality.

Parameter variations		I: the added-phase-control approach		II: the Fourier approach	
Parameter	Sign	RRMSE = 0.045	RRMSE = 0.025	RRMSE = 0.045	RRMSE = 0.025
Defocusing	+	$0.019f$	$0.010f$	$0.00090f$	$0.00050f$
	−	$0.027f$	$0.018f$	$0.0010f$	$0.00050f$
Radius	+	$0.060r_o$	$0.035r_o$	$0.030r_o$	$0.015r_o$
	−	$0.045r_o$	$0.020r_o$	$0.025r_o$	$0.012r_o$
Lateral shift	/	$0.040r_o$	$0.018r_o$	$0.020r_o$	$0.010r_o$

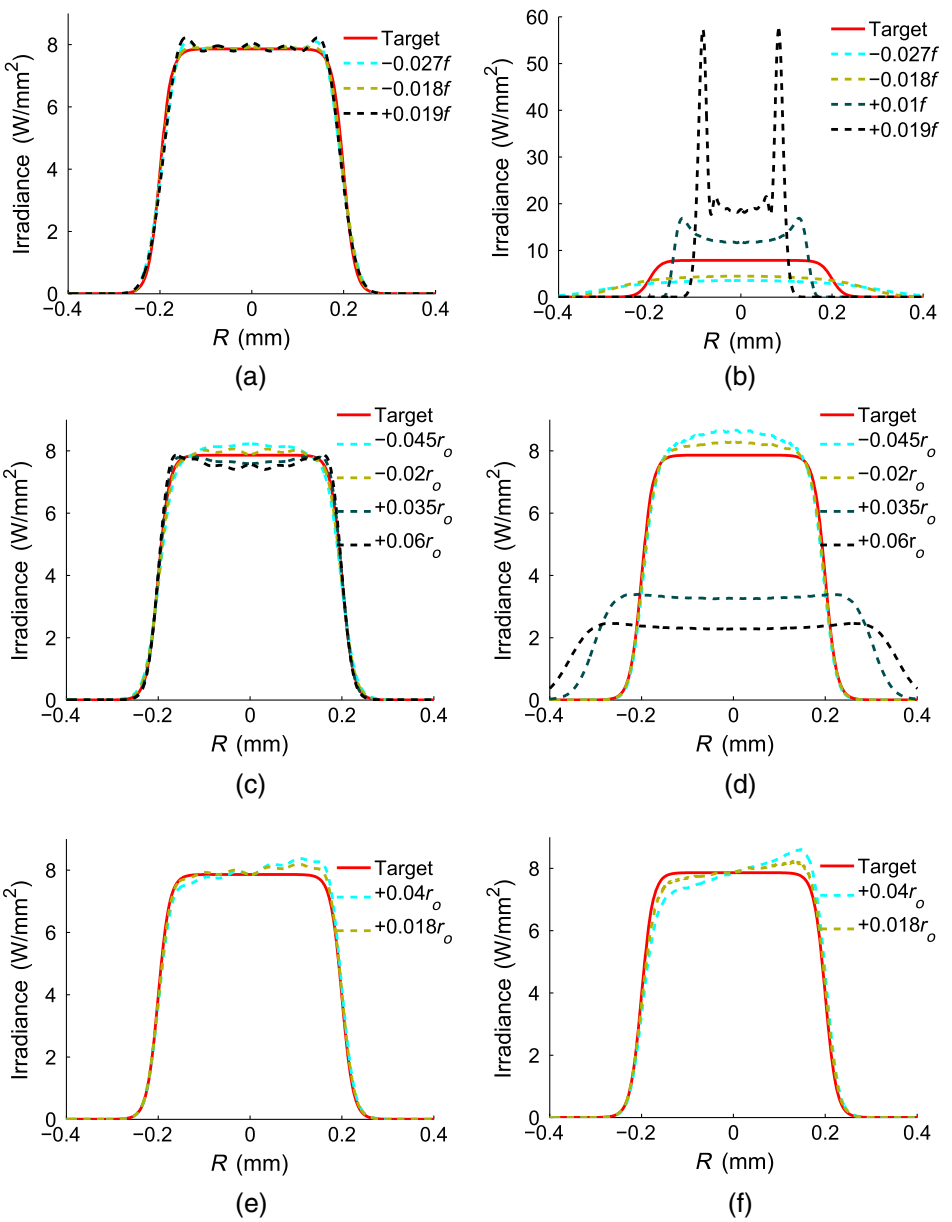

Fig. 7 Simulated irradiance profiles influenced by different parameter variations for the design example in Sec. 3. Results on the left [(a) defocusing 1, (c) radius variation 1, and (e) shift 1] are for the added-phase-control approach, and results on the right [(b) defocusing 2, (d) radius variation 2, and (f) shift 2] are for the Fourier design approach with $\beta = 32$. With the same system imperfections, the obtained profiles are much more deformed for the Fourier approach in comparison with the profiles for the added-phase-control approach.

4.1 *Larger Depth of Focus*

The additional phase control for our approach is expected to provide a large depth of focus, which means that the generated profile can be maintained well within a long distance around the focal plane. The defocusing effects are shown in Fig. 7(a). Defocus is defined such that the detector is not placed at the focal plane. If the detector is placed after the focal plane, the defocusing is positive, otherwise it is negative. Both for the positive and negative defocussing, the deformation of the irradiance profile is similar, with slightly raised-up edges. The only difference is that the design is less sensitive to the negative defocusing, as $-0.027f$ has similar influence as $+0.019f$. Referring to Table 1, both increase RRMSE to 0.045. Hence the depth of focus for a good shaping quality is $0.046f = 12.4$ mm.

In direct comparison, the beam shaper designed with the Fourier approach does not provide an equally good depth of focus. Figure 7(b) shows its defocusing effects. Similar to Fig. 11 of Ref. 10, positive defocusing gives a smaller pattern size, increased average irradiance, and raised-up edges, while negative defocusing produces a larger pattern size and decreased average irradiance. Compared with Fig. 7(a) for the developed design approach, the profile deformation is much larger with the same defocusing. Referring to Table 1, defocusing should not be more than $\sim \pm 0.001f$ to ensure RRMSE smaller than 0.045. The depth of focus is only 511.48 μm which is less than 5% of the value that was achieved with the added-phase-control approach.

4.2 *Less Sensitivity to Input Radius Variations*

The beam shaper is designed for the laser beam with the specified beam size, and the shaping quality is dependent on the size variation. With the same input beam size variations, the obtained irradiance profiles are plotted in Figs. 7(c) and 7(d) for the two designed beam shapers with different approaches, respectively. In both cases, the beam scaling effect is similar to Fig. 10 of Ref. 10, which is that a larger beam size gives raised edges and a smaller beam size rounds off the edges. Compared with the design with the Fourier approach, the design with the added-phase-control approach is less sensitive to the input beam size variation. According to the sensitivity analysis in Table 1, the design with the added-phase-control approach can perform well for the input beam size from 324.7 μm to 360.4 μm, while the design with the Fourier approach is limited from 331.5 μm to 350.2 μm.

4.3 *More Tolerance to the Lateral Shift of the Input Laser Beam*

The lateral shift means that the input laser beam is decentered from the optical axis. The results presented in Figs. 7(e) and 7(f) show that the flattop profile shifts toward the shifting direction, which is similar to the decentering effects in Fig. 9 of Ref. 10. With the same lateral shifts, the design with the added-phase-control approach is able to maintain the profiles much better. As given in Table 1, the tolerance on the lateral shift for the added-phase-control approach is 13.6 μm, which is twice of that for the Fourier approach.

5 Conclusion

Within the scope of this work, we have presented a design strategy and method for FBS based on two plano-aspheric lenses that allow control of both irradiance and phase at focus. This additional phase control at laser focus is realized by combining both geometrical optics and wave optics; an approach that could also prove useful for other laser-based system designs with diffraction effects included. This work demonstrates clearly the added values of the direct phase control at focus. First, unlike the Fourier approach, our approach does not require the use of additional beam expanders to increase the otherwise too low β value. For the example design of transforming Gaussian to a circular flattop pattern at focus, the initial $\beta = 2$ value had to be increased to 32 with a 16× beam expander for the Fourier approach to achieve the shaping quality that is comparable to the result obtained for the two lenses used in our approach. Not only has our developed design approach the potential to yield much more compact optical systems, it also provides a much larger depth of focus, which is more than 20 times longer than that for the design obtained with the Fourier approach. Furthermore, our designed system appears to be less sensitive to the input laser beam, such as the beam size variations and the lateral shifts.

Future work will focus on the generalization to achieve nonrotationally symmetric irradiance patterns at focus using freeform optics and on building a first prototype to verify the results experimentally.

Acknowledgments

The work reported in this paper was mainly funded by an SBO Project Grant 110070, eSHM with AM of the Agency for Innovation by Science and Technology (IWT). It was also supported by the Research Foundation—Flanders (FWO-Vlaanderen) that provides a postdoctoral grant to Fabian Duerr, and in part by the IAPBELSPO Grant IAP P7-35 photonics@be, the Industrial Research Funding (IOF), FWO (G008413N), the MP1205, COST Action, the Methusalem and Hercules foundations, and the OZR of the Vrije Universiteit Brussel.

References

1. F. M. Dickey, S. C. Holswade, and D. L. Shealy, Eds., *Laser Beam Shaping Applications*, CRC Press, Boca Raton (2006).
2. A. Laskin and V. Laskin, "Refractive field mapping beam shaping optics: important features for a right choice," in *Proc. ICALEO 2010*, Paper No. ICA10_M1301 (2010).
3. A. Laskin and V. Laskin, "Applying of refractive spatial beam shapers with scanning optics," in *Proc. ICALEO 2011*, Paper No. ICA11_M604 (2011).
4. F. M. Dickey and S. C. Holswade, Eds., *Laser Beam Shaping: Theory and Techniques*, Marcel Dekker, Inc., New York (2000).
5. L. A. Romero and F. M. Dickey, "Lossless laser beam shaping," *J. Opt. Soc. Am. A* **13**(4), 751–760 (1996).
6. I. Gur and D. Mendlovic, "Diffraction limited domain flat-top generator," *Opt. Commun.* **145**, 237–248 (1998).
7. S. Teng and Z. Liu, "The far-field Gaussian beam shaping under the diffraction limits," *Proc. SPIE* **5525**, 188 (2004).
8. S. C. Holswade and F. M. Dickey, "Gaussian laser beam profile shaping: test and evaluation," *Proc. SPIE* **2863**, 237–245 (1996).
9. N. Hout, N. Sanner, and E. Audouard, "Optimization of the focal volume in programmable spatial beam shaping," *J. Opt. Soc. Am. B* **24**(11), 2814–2820 (2007).
10. F. M. Dickey and S. C. Holswade, "Gaussian laser beam profile shaping," *Opt. Eng.* **35**(11), 3285–3295 (1996).
11. F. M. Dickey, J. A. Hoffnagle, and L. A. Romero, "Gaussian beam profile shaping apparatus, method therefore and evaluation thereof," US Patent, Nr. 5,864,430 (1999).
12. D. L. Shealy, "Optical design of laser beam shaping systems," *Proc. SPIE* **4832**, 344–358 (2002).
13. D. L. Shealy and S.-H. Chao, "Geometric optics-based design of laser beam shapers," *Opt. Eng.* **42**(11), 3123–3138 (2003).
14. J. W. Goodman, *Introduction to Fourier Optics*, 2nd ed., McGraw-Hill Companies, Inc., New York City (1996).

15. J. L. Kreuzer, "Coherent light optical system yielding an output beam of desired intensity distribution at a desired equiphase surface," US Patent, Nr. 3,476,463 (1969).
16. B. R. Frieden, "Lossless conversion of a plane laser wave to a plane wave of uniform irradiance," *Appl. Opt.* **4**(11), 1400–1403 (1965).
17. P. W. Rhodes and D. L. Shealy, "Refractive optical systems for irradiance redistribution of collimated radiation their design and analysis," *Appl. Opt.* **19**(20), 3545–3553 (1980).
18. J. A. Hoffnagle and C. M. Jefferson, "Design and performance of a refractive optical system that converts a Gaussian to a flattop beam," *Appl. Opt.* **39**(30), 5488–5499 (2000).
19. D. L. Shealy and J. A. Hoffnagle, "Aspheric optics for laser beam shaping," in *Encyclopedia of Optical Engineering*, Taylor and Francis, New York (2007).
20. J. A. McNeil, "Design of laser beam shaping optics: a simple algebraic method," *Proc. SPIE* **6872**, 68720D (2008).
21. H. Ma et al., "Improvement of Galilean refractive beam shaping system for accurately generating near-diffraction-limited flattop beam with arbitrary beam size," *Opt. Express* **19**(14), 13105–13117 (2011).
22. Y. Zhang et al., "Double freeform surface design for laser beam shaping with Monge–Ampère equation," *Opt. Commun.* **331**, 297–305 (2014).
23. F. Duerr and H. Thienpont, "Refractive laser beam shaping by means of a functional differential equation based design approach," *Opt. Express* **22**(7), 8001–8011 (2014).
24. M. Li et al., "Comprehensive numerical design approach for refractive laser beam shapers to generate annular irradiance profiles," *Opt. Eng.* **53**(8), 085103 (2014).
25. Z. Feng et al., "Designing double freeform optical surfaces for controlling both irradiance and wavefront," *Opt. Express* **21**(23), 28693–28701 (2013).
26. D. L. Shealy and J. A. Hoffnagle, "Laser beam shaping profiles and propagation," *Appl. Opt.* **45**(21), 5118–5131 (2006).
27. "Nanotech 350FG ultra precision 3-axis freeform generator," http://laser-21.com/moore-tools/ultra-precision/ultra-precision-lathe/nanotech-350fg-ultra-precision-3-axis-freeform-generator/ (1 July 2016).
28. R. Wu et al., "Prescribed intensity design for extended sources in three-dimensional rotational geometry," *Opt. Lett.* **40**(9), 2130–2133 (2015).

Meijie Li received her BS degree in electronics science and technology from Shandong University, China, in 2008. She graduated from the Erasmus Mundus Master program "OpSciTech" in 2010 with a double MS degree, one from Warsaw University of Technology, Poland, and the other one from Delft University of Technology, the Netherlands. She is now a PhD student at Vrije Universiteit Brussel (VUB), Belgium, in optical design and simulation. She is a student member of SPIE.

Youri Meuret graduated in physics in 1998 and received his PhD in applied sciences in 2003, both from Ghent University, Belgium. Afterward, he was responsible for a research group on projection displays and illumination systems in the Department of Applied Physics and Photonics, VUB. Since 2013, he has been an associate professor at the Light and Lighting Laboratory, KU Leuven, Belgium.

Michael Vervaeke has a PhD in electrotechnical engineering on photonic modeling and packaging of chip-level interconnects. He is now responsible for the ultraprecision fabrication technologies for polymer optics and photonic systems at the Brussels Photonics Team. He authored more than 56 publications in international conference proceedings in his research field as well as in education and authored or coauthored more than 11 journal publications.

Hugo Thienpont graduated as an electrotechnical engineer in 1984 and received his PhD in applied sciences in 1990, both from the VUB, Belgium. In 1994, he became a professor at the Faculty of Engineering. In 2000, he became the research director of the Department of Applied Physics and Photonics, VUB, and in 2004, he was elected chair of the department. He is a fellow member of SPIE and EOS, and a member of OSA and the IEEE Photonics Society.

Fabian Duerr graduated in physics from the Karlsruhe Institute of Technology, Germany, in 2008. He then joined the Department of Applied Physics and Photonics, VUB, Belgium, in 2009, where he received his PhD in applied sciences in 2013. As a postdoctoral research fellow of FWO-Vlaanderen, he is currently responsible for a research group that explores the potential of freeform optical designs. He is a member of SPIE and OSA.